Slotless Permanent Magnet Synchronous Motor Operation without a High Resolution Rotor Angle Sensor

Todd D. Batzel and Kwang Y. Lee, *Senior Member, IEEE*

***Abstract*—An implementation for sinusoidal current control of a slotless Permanent Magnet Synchronous Motor (PMSM) with discrete Hall sensor position feedback is presented. To estimate the rotor position of the slotless PMSM, a flux estimation technique is used that takes advantage of the slotless machine's characteristically low inductance to limit flux estimation error. The rotor position is estimated using a reference model and the measured phase currents and voltages. At startup and very low speeds, discrete Hall sensors are used to limit the position estimation error to approximately ± 30 electrical degrees and to prevent the flux estimators from drifting due to measurement noise and offset. The proposed sinusoidal control method reduces the torque pulsations present when Hall sensor position feedback alone is used and eliminates the need for high-resolution rotor angle sensors. The proposed control strategy is applied to a slotless PMSM drive system and implemented using a digital signal processor (DSP). Experiments are carried out for the system and the results demonstrate the effectiveness of the control.**

***Index Terms*—Machine control, permanent magnet synchronous motor, sensorless control, slotless motor.**

I. Introduction

THE DEVELOPMENT and availability of very high-energy density permanent magnet materials has contributed to an increased use of the slotless permanent magnet synchronous motor (PMSM) in high performance applications. The slotless PMSM eliminates rotational cogging torque due to permanent magnet preferred positions, decreases core loss and thus increases efficiency, provides excellent torque-to-volume and power-to-volume ratios, and has a linear current versus torque relation [1].

In the slotless PMSM, in order to generate smooth torque and thus reduce noise and vibration, the current waveform should match the shape of the sinusoidal motor electromotive force (emf) [2]. In order to generate this current waveform, high resolution rotor position feedback is required. This high-resolution rotor position is typically provided by an incremental encoder or resolver attached to the shaft of the motor. Such devices add length and size to the machine, raise system cost, and present reliability issues in harsh environments. As a compromise, Hall sensors, which are installed in the stator by the motor manufacturer, are often used. Hall sensors require little volume in comparison to the resolver or encoder, but provide low-resolution rotor angle feedback—usually 60 electrical degrees resolution. The use of Hall sensors with the slotless PMSM results in a torque ripple and vibration whose frequency is RPM dependent, and thus compromises the low torque ripple inherent to the slotless design [3].

In order to eliminate the need for high-resolution rotor position sensors, many sensorless techniques have been developed for the PMSM. It is well known, however, that sensorless operation is problematic at startup and low-speeds. Several sensorless techniques have been developed for the PMSM to detect the rotor position even at zero speed [4]–[6]. However, these methods rely on rotor saliency and local saturation to detect position, and are not applicable to the slotless machine due to its nonsalient structure and large airgap.

In this paper, an observer will be developed and implemented to derive high-resolution rotor angle information from the slotless PMSM motor phase currents, voltages, and discrete Hall sensor signals. The estimated rotor angle will be used to generate a sinusoidal current waveform and thus reduce torque ripple. The payoff of the proposed technique is the elimination of the high-resolution position sensor without an increase in the torque ripple or a decrease in efficiency. The reduction in size achieved by eliminating the high-resolution rotor position sensor may be critical in many applications.

II. Slotless PMSM Characteristics

In a conventional PMSM, the current-carrying stator windings are held in place by being wound around slots of a stack of steel laminations. Slotless motors eliminate the slots by utilizing windings held together with suitable epoxies.

In Fig. 1, the cross-sections of both a conventional and slotless PMSM are shown. The figure demonstrates that the elimination of the stator teeth from the conventional PMSM provides more space for copper windings in the slotless machine. This higher fill ratio then allows for more magnet surface area, which is required to drive flux across the relatively large airgap. Due to this large airgap, slotless motors have much lower stator inductance—typically $1/10$ to $1/100$ that of conventional machines [7]. Without the stator teeth restricting winding placement, a sinusoidal winding distribution is possible, and a near-perfect sinusoidal back electromotive force (BEMF) results [8]. Thus, in order to generate smooth torque at various operating conditions, the current waveform should be sinusoidal and in phase with the BEMF.

Manuscript received June 16, 1999. This research was supported by the Office of Naval Research under Grant N00014-98-1-0718. NSF provided additional support under Grants INT-9605028 and ECS-9705105.

The authors are with the Department of Electrical Engineering, The Pennsylvania State University, University Park, PA 16802.

Publisher Item Identifier S 0885-8969(00)11011-3.

0885–8969/00$10.00 © 2000 IEEE

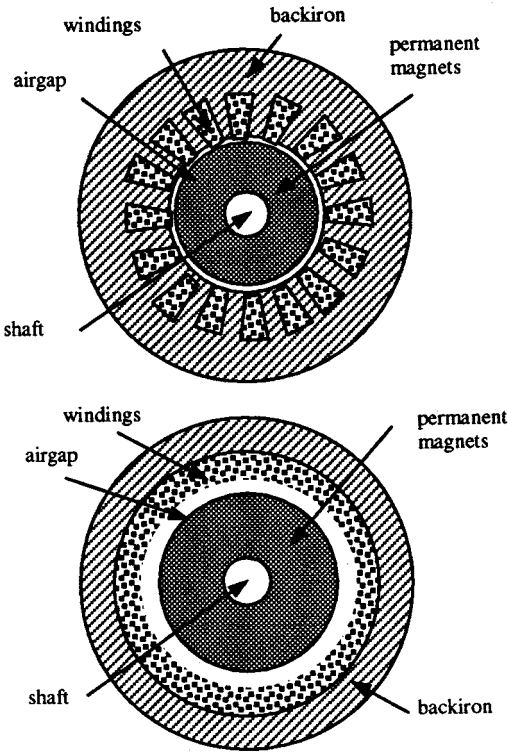

Fig. 1. Cross-section of slotted and slotless PMSM.

The inertia of a slotless PMSM rotor is generally higher than a similarly rated slotted PMSM due to the need for more permanent magnet material in the rotor. The extremely low inductance and relatively high inertia of the slotless machine result in a very wide separation between the mechanical time constant τ_m and the electrical time constant τ_e. This characteristic will be exploited in the development of a sensorless controller for the slotless machine.

Another distinct advantage of the slotless PMSM is its ability to achieve high efficiencies. In slotted motors, stator teeth begin to saturate at operating conditions near rated value. This results in both a decreased efficiency due to core losses and a nonlinear torque per current characteristic. By keeping iron out of the windings, no saturation is present in the slotless machine. This results in decreased iron losses, increased efficiency, and a linear torque per current relation. The linear torque vs. current characteristic is often exploited in servo applications where torque from 5 to 10 times rated value may be used for rapid acceleration.

III. Model of Slotless PMSM

A model for a three-phase PMSM in the stationary reference frame has been developed in [9]. A 2-phase equivalent model in the stationary frame as shown in Fig. 2 is now developed. In this reference frame, the voltages, currents, and fluxes are related to the actual physical quantities by a simple linear transformation often called the Clarke transform [10]:

$$f_{\alpha,\beta,0} = T_c f_{a,b,c}\,; \qquad f_{a,b,c} = T_c^{-1} f_{\alpha,\beta,0} \tag{1}$$

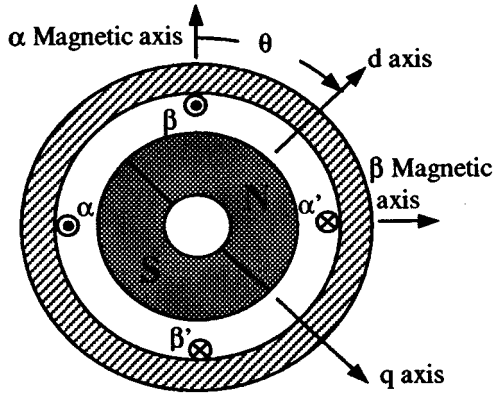

Fig. 2. Equivalent PMSM model in 2-phase stationary frame.

where

$$T_c = \sqrt{\frac{2}{3}} \begin{bmatrix} 1 & -1/2 & -1/2 \\ 0 & \sqrt{3}/2 & -\sqrt{3}/2 \\ \sqrt{1/2} & \sqrt{1/2} & \sqrt{1/2} \end{bmatrix}, \tag{2}$$

$T_c^{-1} = T_c^T$, f represents voltage, current, or flux, and the subscript 0 indicates the zero-sequence component.

The flux equations for the slotless PMSM in stationary coordinates are obtained by applying the Clarke transformation to the corresponding three-phase flux equations, and are given by

$$\begin{bmatrix} \lambda_\alpha \\ \lambda_\beta \end{bmatrix} = \begin{bmatrix} L_l + 1.5L_{ss} & 0 \\ 0 & L_l + 1.5L_{ss} \end{bmatrix} \begin{bmatrix} i_\alpha \\ i_\beta \end{bmatrix} + \sqrt{\frac{3}{2}}\,\lambda_m \begin{bmatrix} \cos\theta \\ \sin\theta \end{bmatrix} \tag{3}$$

and

$$\begin{bmatrix} \dot{\lambda}_\alpha \\ \dot{\lambda}_\beta \end{bmatrix} = \begin{bmatrix} v_\alpha \\ v_\beta \end{bmatrix} - \begin{bmatrix} R & 0 \\ 0 & R \end{bmatrix} \begin{bmatrix} i_\alpha \\ i_\beta \end{bmatrix}, \tag{4}$$

where R, L_{ss}, and L_l represent the per-phase resistance, self-inductance, and leakage inductance, respectively. The terms v, i, and λ with subscripts of α or β represent the voltages, currents, and flux linkages in the equivalent 2-phase model shown in Fig. 2. The superscript $\bullet$ represents the time derivative operator. The zero sequence component is not included in (3) and (4). Solving (3) for the current and substituting the result into (4) yields

$$\begin{bmatrix} \dot{\lambda}_\alpha \\ \dot{\lambda}_\beta \end{bmatrix} = \begin{bmatrix} v_\alpha \\ v_\beta \end{bmatrix} - \frac{R}{L_l + (3/2)L_{ss}} \cdot \left(\begin{bmatrix} \lambda_\alpha \\ \lambda_\beta \end{bmatrix} - \sqrt{\frac{3}{2}}\,\lambda_m \begin{bmatrix} \cos\theta \\ \sin\theta \end{bmatrix} \right). \tag{5}$$

From (5), a state-space form can be obtained. The state vector is defined by

$$x = [\,x_1 \quad x_2 \quad x_3 \quad x_4\,]^T = [\,\lambda_\alpha \quad \lambda_\beta \quad \cos\theta \quad \sin\theta\,]^T, \tag{6}$$

the input vector is

$$u = [\,u_1 \quad u_2\,]^T = [\,v_\alpha \quad v_\beta\,]^T, \tag{7}$$

and the output vector is chosen to be the measurable currents:

$$y = [y_1 \quad y_2]^T = [i_\alpha \quad i_\beta]^T. \tag{8}$$

Thus, the state and output equations are

$$\dot{x} = A_\omega x + Bu \tag{9}$$

$$y = Cx \tag{10}$$

respectively, where

$$A_\omega = \begin{bmatrix} -\tau & 0 & \sqrt{3/2}\lambda_m\tau & 0 \\ 0 & -\tau & 0 & \sqrt{3/2}\lambda_m\tau \\ 0 & 0 & 0 & -\omega_e \\ 0 & 0 & \omega_e & 0 \end{bmatrix}, \tag{11}$$

$$B = \begin{bmatrix} 1 & 0 & 0 & 0 \\ 0 & 1 & 0 & 0 \end{bmatrix}^T, \tag{12}$$

$$C = \begin{bmatrix} \dfrac{\tau}{R} & 0 & -\sqrt{\dfrac{3}{2}}\dfrac{\tau\lambda_m}{R} & 0 \\ 0 & \dfrac{\tau}{R} & 0 & -\sqrt{\dfrac{3}{2}}\dfrac{\tau\lambda_m}{R} \end{bmatrix}, \tag{13}$$

and

$$\tau = \frac{R}{L_l + (3/2)L_{ss}}. \tag{14}$$

The term ω_e represents the angular velocity of the rotor shaft in electrical radians per second. The subscript ω associated with the A matrix indicates that this matrix varies with the angular velocity of the rotor, and is therefore a time-varying system matrix.

IV. Design of Rotor Position Observer

In the design of a rotor position observer for the slotless PMSM, the machine's small electrical time constant relative to the mechanical time constant is exploited. Because of the wide separation between τ_e and τ_m, the rotor velocity is nearly constant throughout each sample period of the position estimation algorithm if the sample period for the position observer is chosen to be fast enough. Thus, it is possible to describe the system's behavior from one sample to the next by using a linear model that is a function of the rotor velocity. This approach suggests the use of two observers—a fast observer for rotor position estimation, and a slower one for the estimation of the angular velocity.

A. Velocity Estimation

To develop an estimator for the angular velocity ω_e, (3) and (4) are used. By assuming the inductance of the slotless machine to be zero, these equations may be manipulated into the following form:

$$\sin\theta = \frac{Ri_\alpha - v_\alpha}{\sqrt{3/2}\omega_e\lambda_m} \tag{15}$$

$$\cos\theta = \frac{-Ri_\beta + v_\beta}{\sqrt{3/2}\omega_e\lambda_m}. \tag{16}$$

The zero inductance approximation is valid given the characteristically low inductance of the slotless PMSM. Consecutively squaring and summing (15) and (16) reveals the estimated magnitude of the angular velocity.

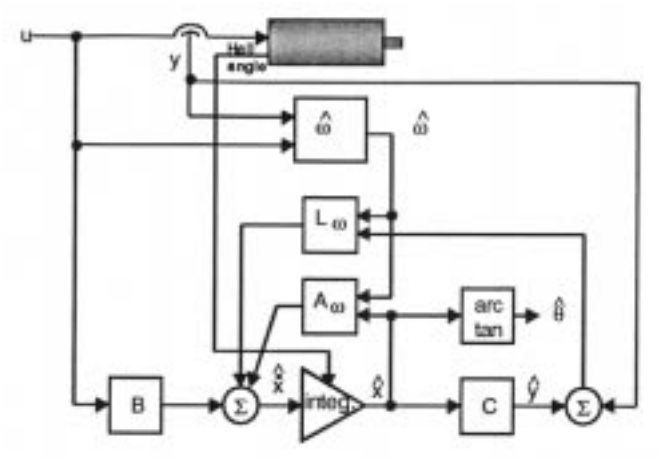

Fig. 3. Block diagram of rotor position observer.

$$|\hat{\omega}_e| = \frac{\left[(v_\alpha - Ri_\alpha)^2 + (v_\beta - Ri_\beta)^2\right]^{1/2}}{\sqrt{3/2}\lambda_m} \tag{17}$$

The sign of $|\hat{\omega}_e|$ is then determined by the direction of rotation of the back emf vector

$$\overline{v}_{\text{emf}} = (Ri_\alpha - v_\alpha) + j\,(v_\beta - Ri_\beta)\,. \tag{18}$$

The estimated velocity $\hat{\omega}_e$ is calculated at a rate much slower than the rotor position estimator, since speed is considered to be a parameter in the position estimator algorithm.

B. Rotor Position Observer

The slotless PMSM system equations of (9) and (10) are now used to design the rotor position observer. It is desired to estimate the state vector x from knowledge of the input vector u and direct measurement of the output vector y. To achieve this, a full order observer is used due to the beneficial smoothing effects that result. Note that if x_3 and x_4 are estimated, the rotor position θ may be calculated by using the relation

$$\tan\theta = \frac{x_4}{x_3} = \frac{\sin\theta}{\cos\theta}. \tag{19}$$

The form of the proposed observer in the sense of Luenberger [11] is

$$\dot{e} = (A_\omega - L_\omega C)\,e \tag{20}$$

where e is the state estimation error vector,

$$e = x - \hat{x} \tag{21}$$

and L_ω is the observer gain matrix. Under the previous assumption that rotor velocity ω is approximately constant over the sample period of the position observer, the system is linear over that period and observable for nonzero rotor velocities. Thus the matrix L_ω can be selected to yield the desired system eigenvalues, and it is then possible to control the rate at which the estimation error e approaches zero. Fig. 3 shows the structure of the resulting observer.

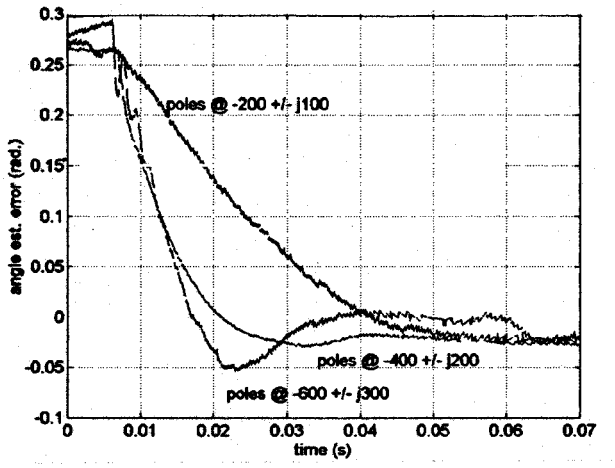

Fig. 4. Rotor angle estimation error convergence for various observer gains.

Each lime a new velocity estimate is available, the observer gain matrix L_ω is calculated by using conventional pole-placement methods [11]. With this technique, the eigenvalues of the characteristic equation

$$|sI - (A_\omega - L_\omega C)| = 0 \tag{22}$$

are placed in the left-half plane at locations such that the observer estimation error e converges to zero within a satisfactory period of time. In Fig. 4, an initial rotor angle error of approximately 15 electrical degrees is introduced to the rotor position estimator. This figure demonstrates that the observer gain matrix show L_ω may be selected to obtain the desired convergence characteristics.

Note that the observer gain matrix is dependent on the rotor velocity, the desired eigenvalues, and the PMSM parameters. Hence, the gain matrix L_ω is scheduled based on the rotor velocity, since the eigenvalues are stationary and the PMSM parameters are assumed to be constant. The eigenvalues of the position observer are chosen so that the position estimation error converges at a fast rate with respect to the rotor speed ω_e. As seen from the estimator, the rotor speed varies slowly enough to be considered as a parameter. At a slower speed, the estimated velocity is calculated using the velocity estimation technique described in the previous section.

As shown in Fig. 3, Hall sensors are used to initialize and bound the integrators corresponding to the state vector x at startup and low-speeds. Under these operating conditions, measurement noise and offsets can lead to integrator drift. At startup, the Hall sensors can provide approximate initial conditions for each integrator.

V. Implementation

A. Experimental System

To evaluate the performance of the proposed rotor position estimator, a set of experiments were performed where the observer was executing the rotor position estimation algorithm in real-time. The estimated rotor angle is provided to the current controller, which generates the sinusoidal current references for each motor phase. The test setup is shown in Figs. 5 and 6.

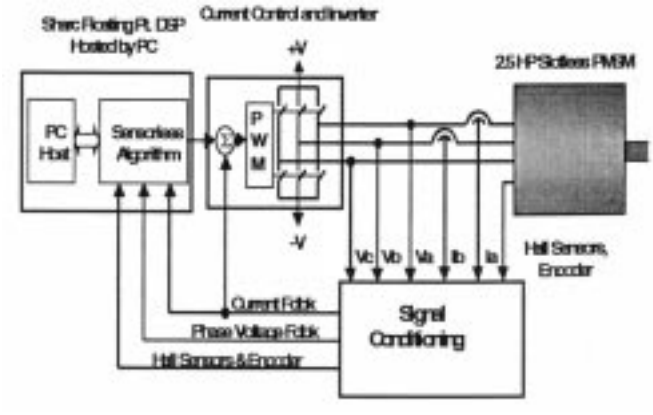

Fig. 5. Block diagram of experiment test setup.

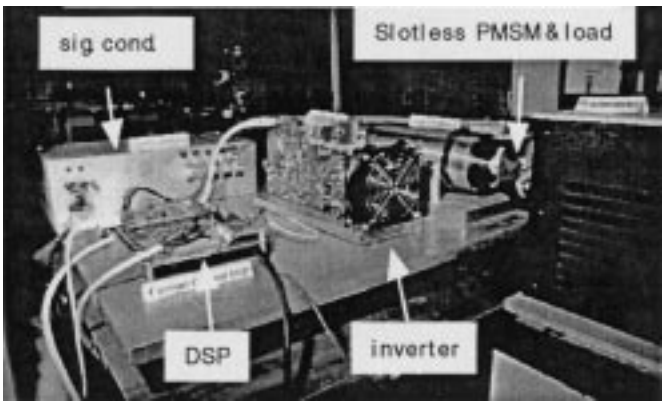

Fig. 6. Experimental test setup.

TABLE I
Parameters of Slotless Motor

Resistance	1.35 Ω
Inductance	.131 mH
Permanent Magnet Flux Linkage	.12 v-s
Poles	4

A floating point digital signal processor (DSP) executes the rotor position estimation algorithm every 50 μs and the velocity estimator every 500 μs. For these experiments, a current controller with PWM switching frequency of 25 kHz was used to drive the slotless motor. The mechanical arrangement consists of a slotless PMSM whose shaft is coupled to a load generator.

B. Experimental Results

Using the test setup depicted in Fig. 6, the rotor position observer performance was evaluated for various steady state and transient operating conditions. The parameters for the slotless machine used in the experiments are given in Table I.

The estimated rotor angle for low speed (50 RPM) steady state operation is shown in Fig. 7. Comparison of the estimated rotor angle with a high resolution encoder attached to the load reveal an estimation error of less than 1.5 electrical degrees. For all experiments, the estimated rotor angle was used to commutate the motor, and the encoder feedback was used only to evaluate the estimation accuracy.

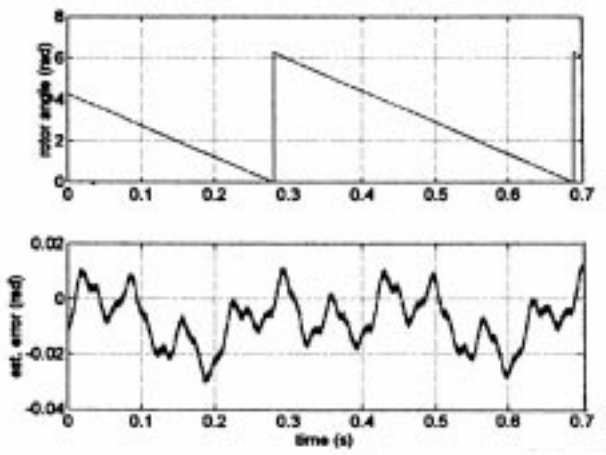

Fig. 7. Actual rotor angle and estimation error at 50 RPM.

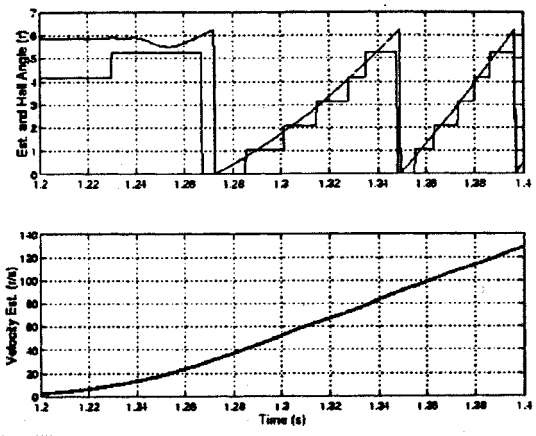

Fig. 8. Rotor position and velocity estimate from zero speed.

Fig. 8 reports the effectiveness of the estimator at startup from zero speed with an initial position error of 100 electrical degrees. The rotor position estimator converges quickly to the correct angle. Note that the initial position error could be normally limited to approximately ± 30 electrical degrees by using the available Hall sensor data to initialize the state vector $\hat{x}$, as shown in Fig. 5.

In Fig. 8, as speed increases, one would expect the Hall sensor transitions to occur at increasingly shorter time intervals. Close examination of the Hall sensor angle data of Fig. 8 indicates Hall sensor installation inaccuracies. This problem is common for the slotless machine due to the absence of stator teeth for sensor alignment and reference. For conventional trapezoidal or six-step current control using the Hall sensors alone, this sensor misalignment would pose problems such as excessive torque ripple, noise, and inefficiency. However, with the rotor position estimator, the sensor alignment is not a factor except at startup and extremely low speeds where the Hall sensors are used.

During speed direction changes, the angular velocity passes through zero speed where position is not observable. Performance of the estimator during a speed reversal is examined in Fig. 9. For this test, the Hall effect sensors were used to commutate the stator currents during operation below the rotor speed

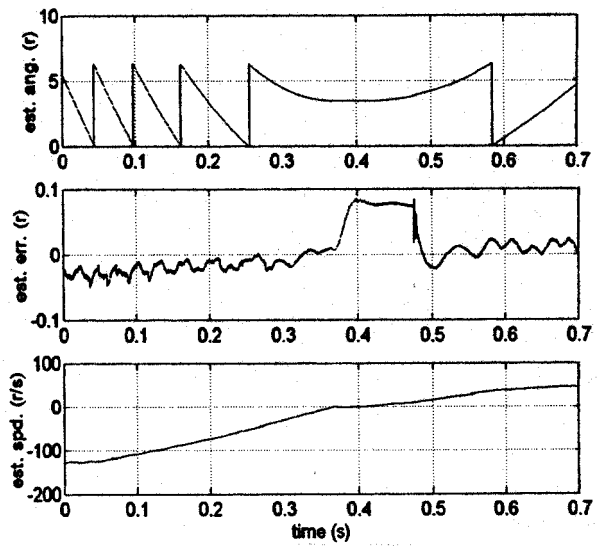

Fig. 9. Rotor position and velocity estimate for speed reversal.

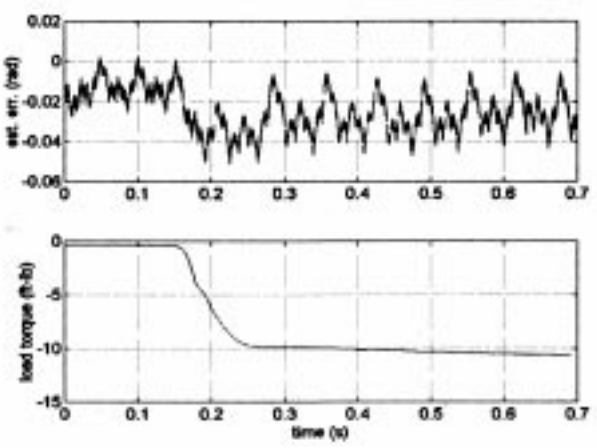

Fig. 10. Estimation accuracy for step load change.

of 10 rad/s. For stability purposes, the observer feedback loop is disabled below the threshold speed.

In Fig. 9, the estimated rotor angle, estimation error, and estimated rotor velocity are shown for the speed reversal condition. Note that while the angular speed is below the threshold of 10 rad/s., the estimated rotor angle error increases since the observer feedback is disabled. At such low speeds where observer performance is limited, the Hall sensor data is used to commutate the motor. When the absolute value of the rotor speed is increased beyond the threshold, observer feedback is restored so that the estimated angle quickly converges toward the actual value. The low-speed threshold was selected such that rotor angle estimation just above the threshold is satisfactory.

In the model described by (5)–(14), there are no mechanical parameters such as load torque or rotor inertia. One advantage of this model is its independence of the mechanical model. In Fig. 10, the rotor estimation accuracy is shown during a step torque change. From this figure, the estimation accuracy is decreased by approximately one electrical degree by the application of the rated torque of the machine.

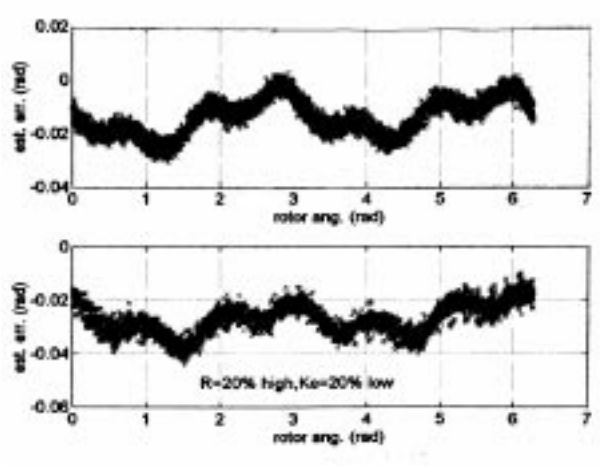

Fig. 11. Estimation error for nominal model and modeling uncertainties.

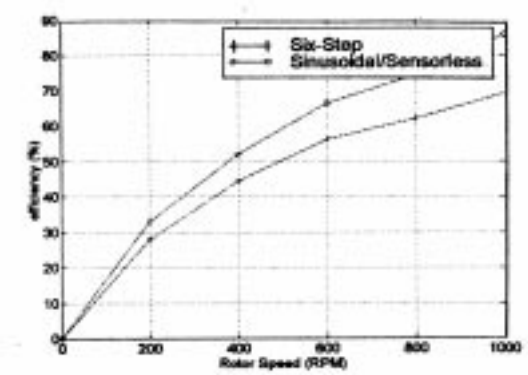

Fig. 12. Machine efficiency for sinusoidal and trapezoidal commutation.

Fig. 11 shows the rotor angle estimation accuracy for the nominal model, and the accuracy for a model in which the actual stator resistance (R) and permanent magnet flux linkage (λ_m) constant are 20% high and low, respectively. These modeling uncertainties were chosen since the stator resistance and permanent magnet flux linkage increase and decrease, respectively, with increasing temperature. This rather severe modeling inaccuracy results in less than one electrical degree of estimation error.

Finally, the efficiency of the slotless PMSM was compared for trapezoidal (six-step) current excitation using only the Hall sensors, and the proposed sensorless sinusoidal drive. The marked improvement in efficiency through use of the sinusoidal algorithm is apparent in Fig. 12.

VI. Conclusion

This paper describes the implementation of a rotor position estimator for a slotless PMSM. Hall sensor data is used to initialize the state vector of the observer at zero speed, where the rotor position is unobservable. At nonzero speeds, the estimator provides high-resolution rotor angle information that may be used to reduce the torque ripple associated with the use of discrete Hall sensor signals as the primary feedback. An experimental setup based on a high-performance DSP has been constructed to evaluate the effectiveness of the proposed observer. Experimental results show that the rotor position estimator performs well under various steady state and transient conditions.

References

[1] J. E. Oliwa, "Custom motor designs with slotless brushless DC motor technology," in *Proceedings, Naval Symposium on Electric Machines*, Newport, RI, July 1997, pp. 157–159.

[2] P. Pillay and R. Krishnan, "Application characteristics of permanent magnet synchronous and brushless DC motors for servo drives," *IEEE Trans. on Ind. Appl*, vol. 27, no. 5, pp. 986–996, Sept.–Oct. 1991.

[3] T. Batzel and K. Y. Lee, "Commutation torque ripple minimization for permanent magnet synchronous machines with Hall effect position feedback," *IEEE Trans. on Energy Conversion*, vol. 13, no. 3, pp. 257–262, Sept. 1998.

[4] N. Matsui and T. Takeshita, "Sensorless control and initial position estimation of salient-pole brushless DC motor," in *International Workshop on Advanced Motion Control: Part 1*, vol. 1, Mar. 1996, pp. 18–23.

[5] T. Aihara, A. Toba, and T. Yanase, "Sensorless torque control of salient pole synchronous motor at zero speed operation," in *Conference Proceedings—IEEE Applied Power Electronics Conference and Exposition*, vol. 2, Feb. 1997, pp. 715–720.

[6] M. Schroedl, "Sensorless control of permanent magnet synchronous motor," *Electric Machines and Power Systems*, vol. 22, pp. 173–185, 1994.

[7] K. Sakai, Y. Tabuchi, and T. Washizu, "Structure and characteristics of new high speed machines with two or three rotor discs," in *Proc. IEEE Industry Applications Meeting*, vol. 1, 1993, pp. 19–26.

[8] T. Batzel and K. Y. Lee, "Sinusoidal commutation of slotless permanent magnet synchronous machines using discrete hall senses feedback," in *Proc. IEEE Power Engineering Society Winter Meeting*, New York, NY, Jan. 1999, pp. 53–58.

[9] ——, "Rotor angle estimation for permanent magnet synchronous machines with hall effect position sensors using neural networks," in *Proc. International Conference on Intelligent Systems Applications to Power Systems*, Seoul, July 1997, pp. 583–587.

[10] E. Clarke, *Circuit Analysis of AC Power Systems*. New York, NY: John Wiley and Sons, Inc., 1943, vol. 1, Symmetrical and Related Components.

[11] W. L. Brogan, *Modern Control Theory*. Englewood Cliffs, NJ: Prentice-Hall, 1991.

Todd D. Batzel received a B.S. degree in electrical engineering from the Pennsylvania State University in 1984, and an M.S. degree in electrical engineering from the University of Pittsburgh in 1989. He is a Research Assistant at the PSU Allied Research Laboratory and a Ph.D. candidate in electrical engineering at the Pennsylvania State University. His research interests include machine controls, electric drives, and power electronics.

Kwang Y. Lee received his B.S. degree in electrical engineering from Seoul National University, Korea, in 1964, his M.S. degree in electrical engineering from North Dakota State University, Fargo, ND, in 1968, and his Ph.D. degree in Systems Science from Michigan State University, East Lansing, MI, in 1971. He has been on the faculties of Michigan State, Oregon State, University of Houston, and the Pennsylvania State University, where he is currently a Professor of Electrical Engineering. He is Director of Power Systems Control Laboratory, and a Co-Director of Intelligent Distributed Controls Research Laboratory at Penn State. His interests include control systems, artificial intelligence, neural networks, fuzzy logic control, genetic algorithms, and their applications to power plants and power systems control, operation and planning. He is a Senior Member of IEEE, active in Power Engineering Society and Control Systems Society.